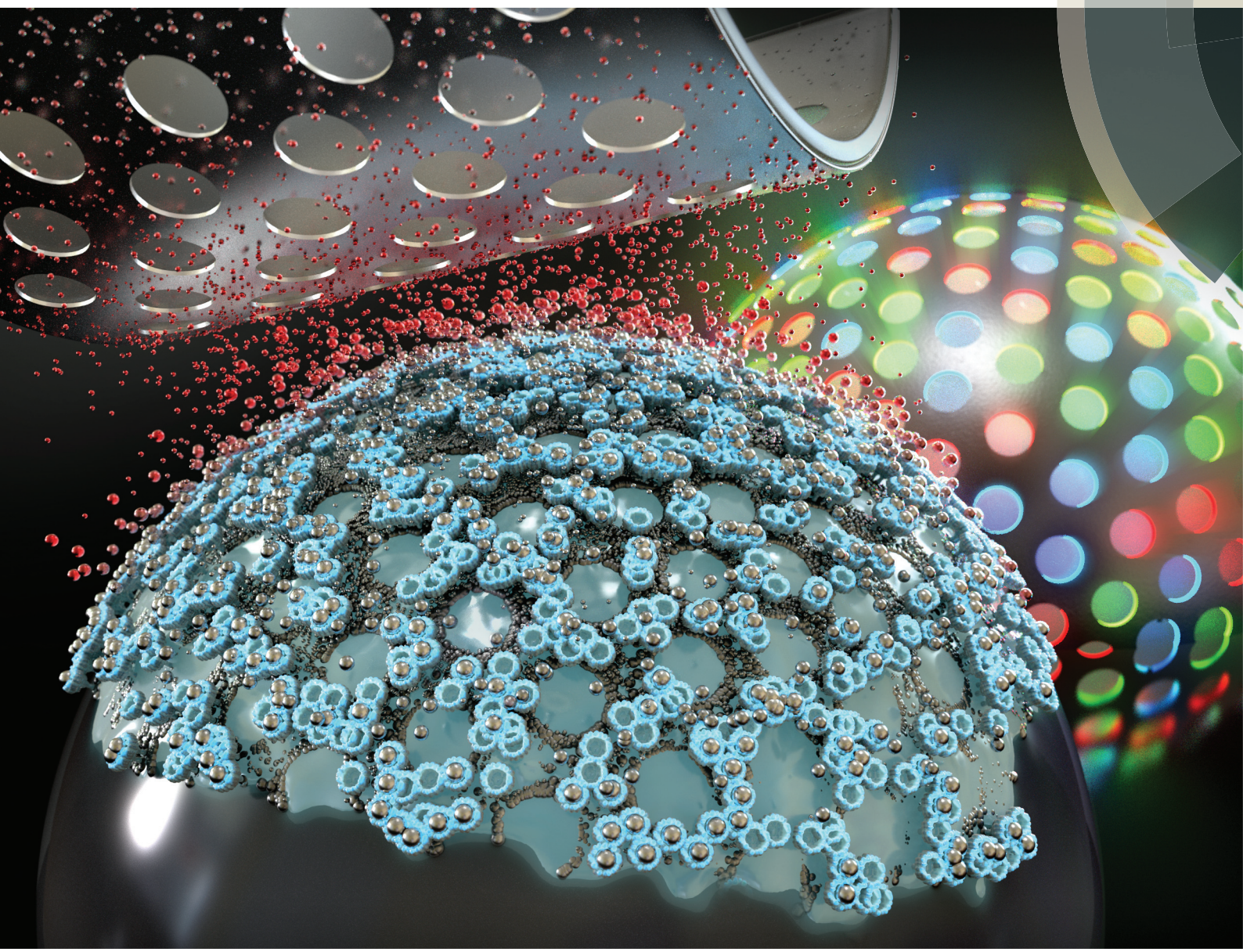
Volume 11 | Number 23 | 21 June 2019 | Pages 11035–11382

Nanoscale

rsc.li/nanoscale



ISSN 2040-3372

ROYAL SOCIETY OF CHEMISTRY | Celebrating IYPT 2019

PAPER
Jun Ho Jeong *et al.*
Repeatable and metal-independent nanotransfer printing based on metal oxidation for plasmonic color filters

NCNST

Published on 26 April 2019. Downloaded by Korea Advanced Institute of Science & Technology / KAIST on 11/21/2022 1:33:02 PM.

Nanoscale

PAPER

View Article Online
View Journal | View Issue

Check for updates

Cite this: *Nanoscale*, 2019, **11**, 11128

Repeatable and metal-independent nanotransfer printing based on metal oxidation for plasmonic color filters†

Soon Hyoung Hwang, Zhi-Jun Zhao, Sohee Jeon, Hyeokjung Kang, Junseong Ahn and Jun Ho Jeong *

Received 7th January 2019,
Accepted 25th April 2019

DOI: 10.1039/c9nr00176j

rsc.li/nanoscale

Many recently developed nanotransfer printing techniques have received much attention because of their simplicity and low cost. In addition, such techniques are suitable for fabricating nano/microscale sensors, optical elements, and electrical devices. However, conventional nanotransfer printing methods are time-consuming, cannot be easily used over large areas or with several different materials, and are not suitable for repeatedly transferring various materials onto the same substrate or a curved surface. Herein, a new nanotransfer printing method is introduced based on the oxidation of various metals and the formation of covalent bonds between spin- and spray-coatable adhesives and the chosen metal at low temperatures. These strong covalent bonds allow the fast transfer of the deposited materials from a polymer stamp without additional processing. A major advantage of this process is that it is metal-independent; nanowires of various metals are successfully transferred from the polymer stamp because strong covalent bonds form instantaneously between the metal and an adhesive-coated substrate. Moreover, this nanotransfer process can be used repeatedly to fabricate large-scale color filters from smaller areas of nanowires, regardless of the metal type and nanostructure orientation. Furthermore, plasmonic color filters composed of nanohole arrays can be obtained on both flat and curved surfaces.

1. Introduction

Many high-resolution techniques for fabricating nano/microscale structures have been developed, including electron-beam lithography (EBL),[1–4] laser direct writing (LDW),[5–8] nanoimprint lithography (NIM),[9–12] and nanotransfer printing (nTP).[13–16] These techniques have been demonstrated for nano/microscale applications, such as electrical devices,[17,18] sensors,[19–21] microfluidics devices,[22,23] and optical elements.[24–27] Among the various fabrication techniques, EBL has the capability of fabricating high-resolution (<10 nm) patterns and is not limited in the pattern shape over a large area; however, it is an expensive, time-consuming, and complicated process, and changing the material is difficult during the process.[28,29] The LDW method can also fabricate high-resolution three-dimensional nano/microscale patterns by directly patterning the photoresist.[30,31] However, LDW is also time-consuming and difficult to apply over large areas. It is well known that NIM is a simple and cost-effective method for fabricating nano/microscale patterns. However, a major disadvantage of this method is the development of non-uniform residual layers that need to be removed by additional processes, such as reactive ion etching (RIE) or lift-off processes, in order to etch the target material.[32,33] In addition, it is difficult to remove the residual layer uniformly over a large area and apply this to different substrate materials.

The nTP technique has received much attention as it can overcome many of these challenges. The nTP method takes advantage of the differences in relative bonding strengths between the material to be transferred and a stamp (often made of polydimethylsiloxane (PDMS) or an imprint resin) and that between the material and a receiving substrate. Therefore, it is essential to control the bonding strength in order to detach the target materials successfully. In addition, transferring target materials to the substrate without a residual layer is a significant advantage of nTP that makes it more simple and easy to use than NIM. Although nTP can be used to transfer materials in a simple and cost-effective manner,[34–37] there are several issues that need to be addressed. For example, there are limitations related to select-

Nano-Convergence Mechanical Systems Research Division, Korea Institute of Machinery and Materials, Daejeon 34103, South Korea. E-mail: jhjeong@kimm.re.kr

†Electronic supplementary information (ESI) available: Additional TEM images, FIB images, photographic images, and XPS spectra, and the color filter conceptual design. See DOI: 10.1039/c9nr00176j

This journal is © The Royal Society of Chemistry 2019

Published on 26 April 2019. Downloaded by Korea Advanced Institute of Science & Technology / KAIST on 11/21/2022 1:33:02 PM.

ing and changing materials. In addition, it is difficult to repeatedly fabricate nano/micropatterns made of distinct materials on the same substrate, and the use of curved surfaces is complicated.

Several research groups have attempted to overcome these difficulties in order to promote the widespread use of nTP. For example, Seo *et al.* proposed mechanical-interlocking-based nTP to transfer nanowires of various materials (Au, Pt, Cu, and Cu_2O) by etching an amorphous carbon nanosacrificial layer.[38] Tiefenauer *et al.* developed a nanotransfer method based on template stripping with nTP and transferred nanopatterns on a curved substrate by dissolving the stamp mold.[39] Hwang *et al.* successfully transferred various materials, including metals and inorganic materials (SiO_2), using the covalent bonding between the oxygen of SiO_2 and Si of the adhesive layer, and demonstrated a metasurface and wire grid polarizer.[40] Several researchers have used (3-aminopropyl)triethoxysilane (APTES) and (3-mercaptopropyl)trimethoxysilane (MPTMS) to transfer Au to substrates such as PDMS by employing the covalent boding between Au and APTES amine groups and MPTMS thiol groups.[41–44] However, such methods provide only partial solutions, *e.g.*, are suited for the transfer of nanowires of various materials, transfer of Au to curved substrates and PDMS, and the fabrication of optical elements. Moreover, these techniques involve complicated processes such as dry etching, require two-fold transfer of the target material, and rely on the presence of SiO_2 (providing oxygen for the adhesive layer) on the polymer stamp. Finally, transfer protocols based on the use of APTES and MPTMS can only be applied to Au and require a long time for the deposition of the adhesive layer on the substrate. Moreover, these methods are not suitable for repeatedly transferring materials using the same substrate, as processes such as dry etching and dissolving the stamp in water can damage the transferred materials.

To address these challenges, we took advantage of two properties of metal nanopatterns, namely, they can be (i) melted and welded at relatively low temperatures (~100 °C), unlike bulk metals,[45] and (ii) naturally oxidized during deposition. Hence, nanoscale metals can produce either cation states or oxidized states, which can form robust and instantaneous covalent bonds with silicon- and oxygen-containing adhesives without the need for oxide materials or additional processes. We investigated a transfer method based on this mechanism and tested whether it was possible to detach deposited metals from a nanopatterned polymer stamp and transfer them to flat and curved surfaces. We investigated the dependence of the transfer printing method on the metal type using various metals (Ag, Au, and Al). In addition, we investigated the use of a stitch process, whereby we sequentially transferred nanopatterns side-by-side to fabricate large-area color filters by repeatedly transferring patterns from a smaller polymer stamp. In order to verify the process for real applications, we fabricated a plasmonic color filter composed of nanohole arrays and evaluated the quality of the transfer on both flat and curved substrates.

2. Experimental

2.1. Materials

Si masters with nanohole and line patterns were fabricated using a KrF lithography process. Self-assembled monolayers (SAMs) were formed on the surface of the fabricated Si master using trichloro(1*H*,1*H*,2*H*,2*H*-perfluorooctyl)silane at 80 °C for 30 min. An ultraviolet (UV)-curable imprint resin (RM-311; Minuta Technology Co., Ltd, Korea) and Ormo-stamp (MicroResist Technology, Germany) were used. To prepare the polymer stamp, the imprint resin was dropped onto the surface of the Si master and covered by a polyethylene terephthalate (PET) film; then, pressure was applied to fill the nanopattern of the Si master with resin. Subsequently, the Si master, imprint resin, and PET film were UV-cured for 90 s. After curing, the imprint resin and PET film were peeled off the Si master and cured again under UV for 90 s. The replicated polymer stamp was subjected to SAM treatment in the same way as the Si master.

Three different metals (Au, Ag, and Al) were deposited on the polymer stamp using electron beam evaporation (Daeki Hi-Tech Co., Ltd, Korea) at a deposition rate of 1 Å s^{-1}. *N*-[3-(Trimethoxysilyl)propyl]ethylenediamine was used as an adhesive material. Propane-1,3-diol and di(propylene glycol) methyl ether were used as solvents. All materials were purchased from Sigma-Aldrich. The adhesive material and solvents (volume fractions of 1%, 70%, and 29%, respectively) were mixed under ultrasonication for 30 s.[40]

2.2. Substrate preparation

Si and glass wafers were plasma treated to enhance the hydrophilicity of the substrate surface. The adhesive solution was dropped on the surface of substrate and spin-coated for 60 s at 5000 rpm. Then, the substrate was baked for 60 s at 150 °C to evaporate the solvents. The adhesive solution was coated on the cured substrate using spray coating for 10 s and baked at 150 °C in an oven for 5 min to evaporate the solvents.

2.3. Characterization

X-ray photoelectron spectroscopy (XPS; K-Alpha+, ThermoFisher Scientific, USA), with an ion gun operated under conditions of 500 eV, 10 mA, and monoatomic Ar^+, was employed to determine the Ag, Au, and Al binding energies. The angle between the X-ray gun and electron energy analyzer was about 45°, while the electron energy analyzer was placed normal to the prepared sample surface. The Au, Ag, and Al layers, both with and without nanopatterns, were transferred to adhesive-coated Si wafers at 150 °C. In addition, the polymer stamp with the deposited metal layer was also analyzed by XPS both with and without nanopatterns. Each sample was etched downward over an area of 200 × 200 μm^2 to obtain the binding energy of different metals at the metal–adhesive and metal–polymer stamp interfaces. A focused ion beam (FIB; Helios Nanolab, FEI, USA) system, scanning electron microscopy (SEM; JSM-7800F, JEOL, Japan), and transmission electron microscopy (TEM; JEM-ARM200F, JEOL,

Published on 26 April 2019. Downloaded by Korea Advanced Institute of Science & Technology / KAIST on 11/21/2022 1:33:02 PM.

Japan) were employed to obtain high-resolution surface and cross-sectional images of the samples. Images of the fabricated color filter were obtained using optical microscopy (Eclipse LV 100, Nikon Instruments, Inc., USA) using the unpolarized output from a halogen lamp as a light source.

2.4. Calculations

The finite-difference time-domain (FDTD) method was used to calculate transmittance and reflectance spectra in the visible region in order to design the geometry of the color filter and compare the results with experimental observations. Commercial FDTD software (Lumerical FDTD Solutions 8.19.1541, Lumerical Inc.) was used with a total simulation window of $a \times \sqrt{3}a \times 1800$ nm^3, where a is the lattice constant, and periodic ($\pm x$, $\pm y$ directions) and perfect matching layers ($\pm z$ direction) were used as boundary conditions. The plane wave in the 380–830 nm range was propagated perpendicular to the nanostructured plane as the light source. The mesh sizes were set as $2 \times 2 \times 2$ nm^3, where 2 nm was less than 1/200 of the wavelength. The measured refractive index of each material was used for calculation. The transmittance and reflectance were observed in the x–y plane, ~1000 nm away from either side of the nanostructured layer.

3. Results and discussion

3.1. Repeatable metal-independent nTP

The process developed in this study, hereafter referred to as metal-independent nTP (MiNP), is shown schematically in Fig. 1. The polymer stamp was prepared using standard procedures, as described in the Experimental section. Various metals (Au, Al, and Ag) were deposited using electron beam evaporation on the prepared flexible polymer stamp containing a nanopattern with line (L) and spacing (S) values both of 100 nm (100 nm L/S). After evaporating the solvents, during the nTP process at 150 °C, Au and Ag in contact with the adhesive layer formed cation states, whereas Al was oxidized

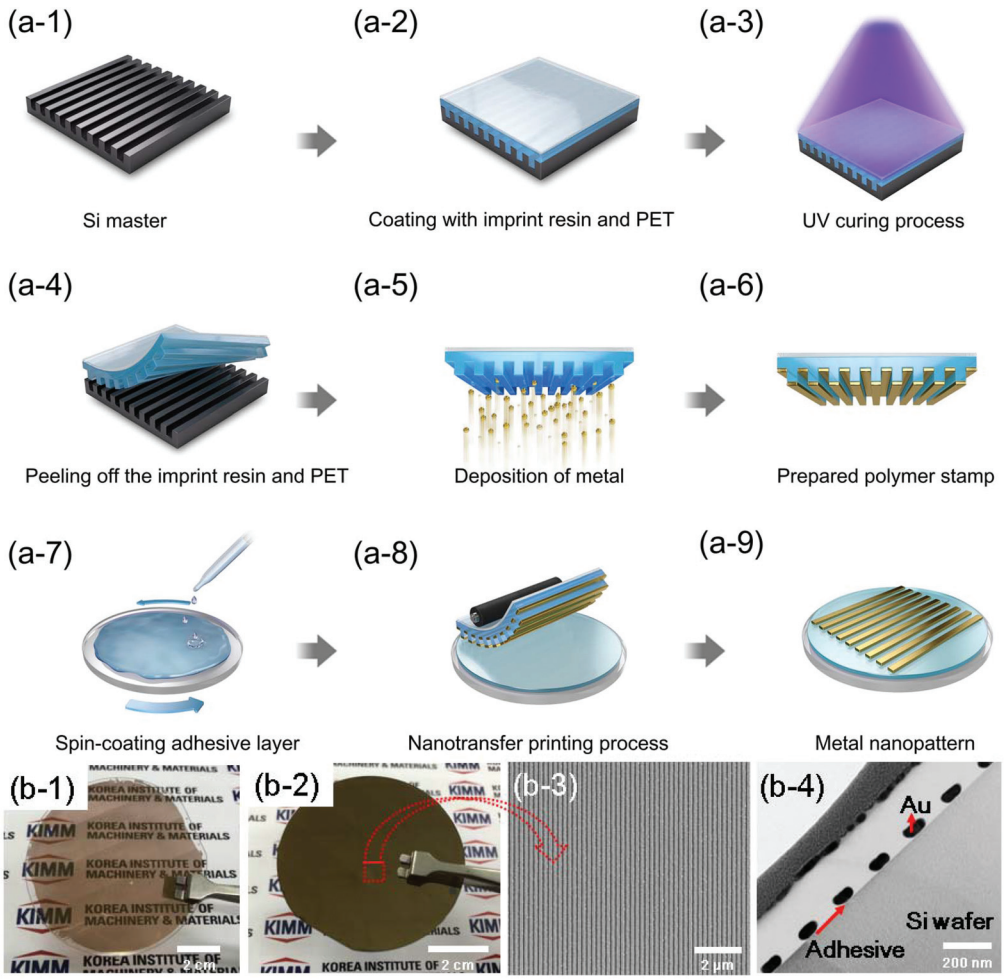


Fig. 1 (a) Schematic diagram of the MiNP process *via* metal oxidation. (a-1) Si master with nanopattern; (a-2) coating with UV-curable imprint resin and covering with a PET film; (a-3) UV curing; (a-4) peeling off replicated flexible polymer stamp from the Si master; (a-5) metal deposition on the polymer stamp; (a-6) prepared polymer stamp with deposited metal; (a-7) spin-coating adhesive layer; (a-8) nTP step; and (a-9) final nanopattern transferred to the substrate. (b) Photographs of metal-transferred (1) glass and (2) Si substrates (2 inch diameter), and (3) surface FIB image and (4) cross-sectional TEM image of transferred 100 nm L/S nanopatterns of Au.

 This journal is © The Royal Society of Chemistry 2019

Published on 26 April 2019. Downloaded by Korea Advanced Institute of Science & Technology / KAIST on 11/21/2022 1:33:02 PM.

during deposition. As a result, Au and Ag formed covalent bonds with oxygen in the adhesive and the Al oxide formed covalent bonds between its oxygen atoms and Si in the adhesive; this mechanism is discussed in detail in section 3.2. As shown in the surface and cross-sectional FIB and TEM images (Fig. 1(b) and Fig. S1†), the metals formed chemical bonds with the adhesive material, resulting in metal nanowires (Au, Ag, and. Al) with widths of 100 nm being successfully transferred to 2 inch diameter glass and Si wafers. The photographs show that we successfully transferred various metals using the fast MiNP method, producing nanowires without defects.

An advantage of the proposed method is that it is possible to sequentially transfer various nanopatterns made of different metals onto the same substrate, regardless of the orientation of the patterns. This is particularly relevant for hologram applications, where the required metasurface with various orientations of angular nanorods[46,47] is difficult to fabricate using EBL or FIB over a large area, but could be fabricated using the MiNP process.

As shown in Fig. 2(a), the liquid adhesive can be repeatedly coated on the substrate onto which the Au nanowires were transferred; then, other metal nanowire patterns can be transferred to the same substrate. The adhesive layer is transparent, with a thickness of a few nanometers (Fig. S2(a-2)†); therefore, it is considered that it does not influence the transferred nanowires. To verify this method, three polymer stamps with 100 nm *L*/*S* were prepared following the procedure shown in Fig. 1. One of these polymer stamps was placed below a mask with fixed orientation and Au was deposited through the mask. Another polymer stamp was placed below the mask (diagonally with respect to the first polymer stamp) and Ag was deposited. The third stamp was then placed below the mask (perpendicular with respect to the first polymer stamp) and Au was deposited. All polymer stamps with metals had the same pattern as the mask shown in Fig. S3;† however, each had a different orientation and metal. In the second step, the adhesive layer was coated on a 6 inch wafer and 100 nm Au nanowires with vertical orientation were transferred onto the substrate (Fig. 2(b) and (d-1)). Next, another adhesive layer was coated on the substrate and 100 nm Ag nanowires with diagonal orientation were transferred onto a different area of the same substrate (Fig. 2(b) and (d-2)). Lastly, another adhesive layer was coated on the same substrate, and 100 nm Au nanowires with perpendicular orientation were transferred (Fig. 2(b) and (d-3)). Each of the line patterns shown in Fig. 2(b) were formed with different metals and orientations, as shown by the different colors under linearly polarized light (Fig. S4†). Fig. 2b shows photographs of Au nanowires under (Fig. 2d-1 and d-3) 45° linearly polarized light and (Fig. 2d-2) parallel linearly polarized light. The surface and cross-sectional FIB images in Fig. S5† show that the patterns with different metals and orientations were successfully transferred onto the substrates. A critical factor in this method is that the binding energy between the oxidized metal and adhesive layer should be stronger than that between the polymer stamp and oxidized metal. This relative difference in binding energies allows the deposited material to be transferred to the adhesive-coated substrate from the polymer stamp. However, the Ag nanowires (Fig. 2b) showed some defects due to contamination with particles during the metal deposition and transfer process. Fig. S4d and S4e† show that the formed covalent bonding was strong enough to remove deposited materials from the polymer stamp, which does not necessarily mean that the bonding energy between the Ag nanowires and adhesive layer is lower than that between the Au nanowires and adhesion layer.

Another significant advantage of the MiNP process is the ability to stitch together nanopatterns (with different materials and/or orientations) on the same substrate. The stitch method was performed using the metal-deposited polymer stamps. The metal nanowire pattern from the polymer stamp was transferred to the substrate. Then, an adhesive layer was coated onto the same substrate and another metal pattern was transferred from a polymer stamp close to the edge of the previously transferred metal nanowire pattern. This sequential nanotransfer allowed nanopatterning over a large area. Therefore, it was possible to fabricate large-area devices, such as color filters, with different materials (Fig. 2(c)). In addition, it was possible to fabricate a wire grid polarizer using the small area of the prepared samples. Fig. 2(c) shows photographs of a sample fabricated using Au and Al nanowires transferred using MiNP and combined using the stitch method, and its color with respect to the angle of linearly polarized light is shown in Fig. S6.† In this case, 100 nm *L*/*S* polymer stamps coated with Al and Au were prepared, and then the metals were sequentially transferred onto the same glass substrate, resulting in the structures shown in Fig. 2(e). The gap between the transferred Al and Au patterns was ~17.5 μm, which is small enough to provide functionality as an optical element, such as a color filter. It is worth noting that in addition to parallel line patterns, it was possible to stitch nanopatterns with diagonal and vertical orientations, as shown in Fig. 2(f). However, some rough edges were observed in Fig. 2(f-2), which were formed during the sequential transfer process as the metal nanowires on the polymer stamp could not come in contact with the adhesive and disconnected owing to previously transferred metal nanowires. This issue could be addressed by applying higher pressure during the sequential transfer process to ensure that there is good contact between the nanowires and adhesive layer. It is expected that large-area nanostructures can be fabricated using MiNP by stitching together small areas of patterns with various orientations and materials.

3.2. Adhesion mechanism

To analyze the mechanism of adhesion occurring between the metal and adhesive during MiNP, we conducted an XPS analysis of transferred 100 nm *L*/*S* nanopatterns made of Ag, Au, and Al on Si substrates (Fig. 3). The Au, Ag, and Al layers, both with and without nanopatterns, were transferred onto adhesive-coated Si wafers at 150 °C. All of these metals were

Published on 26 April 2019. Downloaded by Korea Advanced Institute of Science & Technology / KAIST on 11/21/2022 1:33:02 PM.

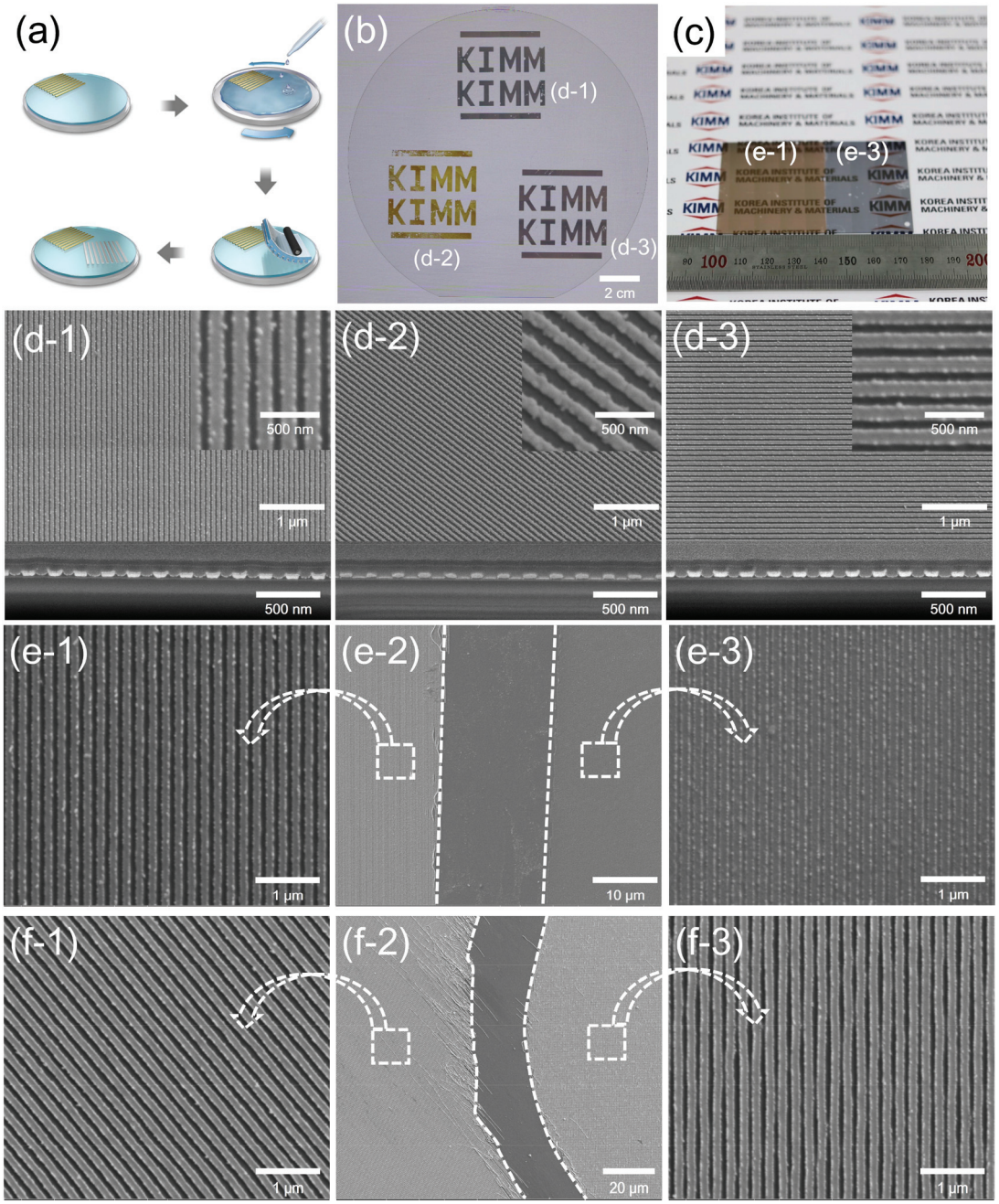


Fig. 2 (a) Schematic diagram showing the repeatable MiNP process. (b) Photographs of Au and Ag nanowires with different orientations transferred three times onto the same substrate. (c) Photographs of stitched Al and Au nanowires. Surface and cross-sectional SEM images with different magnifications of transferred (d-1) Au nanowires, (d-2) Ag nanowires with diagonal orientation with respect to (d-1), and (d-3) Au nanowires with perpendicular orientation with respect to (d-2). (e) Surface FIB images of (c): transferred (e-1) Au nanowires, (e-2) stitch area, and (e-3) Al nanowires; (f-1) Au nanowires with diagonal orientation with respect to (f-3), (f-2) stitch area, and (f-3) Au nanowires.

deposited on the polymer stamp with 100 nm *L*/*S* nanopatterns and transferred to adhesive-coated Si wafers (Fig. 3). In addition, the different metals were deposited on the polymer stamp without nanopatterns and transferred to adhesive-coated Si wafers as thin films (Fig. S8, S10 and S12†). Furthermore, the metals were deposited on the polymer stamp with 100 nm *L*/*S* nanopatterns, and without nanopatterns (Fig. S8–S12†). All of these twelve types of prepared samples were analyzed using XPS. Each sample was etched downward from the surface over an area of 200 × 200 μm^2 using the XPS electron flood gun to obtain the binding energy of different metals at the metal–adhesive and metal–polymer stamp interfaces. In this study, it was essential that metal cations were present (Ag and Au) or that the metal oxide provided oxygen atoms to the adhesive (Al) at the interface to form covalent bonds. Nanostructured metals can be melted and oxidized at

 This journal is © The Royal Society of Chemistry 2019

Published on 26 April 2019. Downloaded by Korea Advanced Institute of Science & Technology / KAIST on 11/21/2022 1:33:02 PM.

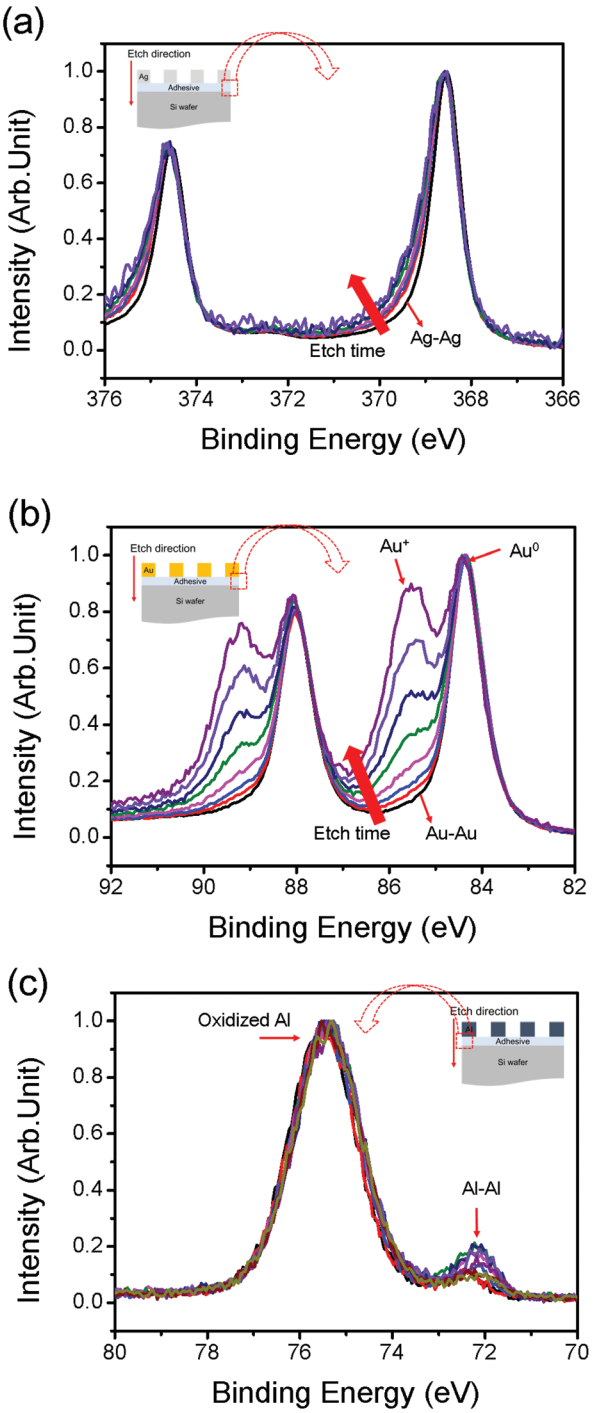


Fig. 3 XPS profiles showing normalized binding energy intensities of (a) Ag, (b) Au, and (c) Al at different etch times during etching of the multilayer structure. The inset illustrations show the sample structure.

lower temperatures than bulk metals. For example, nanoscale Ag can be meted at 100 °C;[45] therefore, annealing of the substrate was performed at 150 °C during the MiNP process. The binding energy spectra and atomic concentrations for each sample are presented in Fig. 3 and Fig. S7–S12.† The processing temperature was sufficient to melt the nanoscale Ag and form cations, which facilitated the formation of covalent bonds with oxygen from the adhesive layer, yielding AgO_x. The XPS profiles of Ag in Fig. 3(a) show that the binding energy peak of Ag broadens as the etching time increases. The full width at half maximum (FWHM) of the Ag $3d_{5/2}$ peak was 0.78 eV, whereas that of the oxidized Ag $3d_{5/2}$ peak was broader (1.03 eV);[48] the value for oxidized Ag $3d_{5/2}$ value is in good agreement with that previously reported.[49] Considering these results, we concluded that the Ag^0 state transformed into the Ag^+ state and formed covalent bonds with oxygen from the adhesive to give Ag_2O at the metal–adhesive interface. We also measured the binding energy of Ag deposited on the polymer stamp before transfer to the substrate; in this case, no peak broadening was observed (Fig. S7 and S8†). The Ag on both the polymer stamp and the top layer on the substrate after MiNP showed typical binding energy spectra of Ag. The XPS profiles verified that the nanostructured Ag at the metal–adhesive interface formed covalent bonds, which was the reason for successful transfer of the metal to the substrate.

In the case of Au, the XPS profile indicated that the top of the transferred layer (away from the interface) showed a typical binding energy spectrum, with the Au $4f_{7/2}$ peak having a binding energy of 84.38 eV. However, as the etch time increased, Au^+ exhibited a peak at 85.53 eV, as shown in Fig. 3(b),[50] at the interface between the adhesive layer and the Au nanopattern at 150 °C. This binding energy of Au indicated that Au changed to the oxidized Au^+ state and formed covalent bonds with oxygen from the adhesive layer to give AuO^-. When the Au pattern was not annealed, these changes were not observed, as shown in Fig. S9(b) and S10(b).† These spectra showed the typical Au binding energy, indicating that Au did not change into Au^+. The covalent bonding was stronger than the bond strength between the polymer stamp and the deposited Au, enabling successful transfer of Au from the polymer stamp to the adhesive-coated substrate. In addition, when Ag and Au were deposited on the polymer stamp as thin films (without a pattern), the metals at the interface with the adhesive were oxidized, and the obtained cation states formed covalent bonds with oxygen (Fig. S8 and S10†).

It is well known that Al metal can be easily oxidized. As shown in Fig. 3(c), the XPS profile of a transferred Al nanopattern on a Si wafer possesses two peaks corresponding to oxidized Al 2p (75.23 eV) and Al 2p metal (72.18 eV).[51,52] In addition, the peak of oxidized Al is much more intense than the metal Al peak, indicating that many oxygen atoms are available for the adhesive and to form covalent bonds with Si within the adhesive layer without oxide materials.

3.3. Fabrication of a color filter using MiNP on curved surfaces

Various fabrication techniques have been reported to achieve color using nanostructures. Various colors can be realized by depositing metal and dielectric materials on the polymer stamp (*e.g.*, as shown in Fig. 1(a-6));[53] however, materials are deposited on both the line and space area of the polymer stamp, so the transmittance of the incident light could

Published on 26 April 2019. Downloaded by Korea Advanced Institute of Science & Technology / KAIST on 11/21/2022 1:33:02 PM.

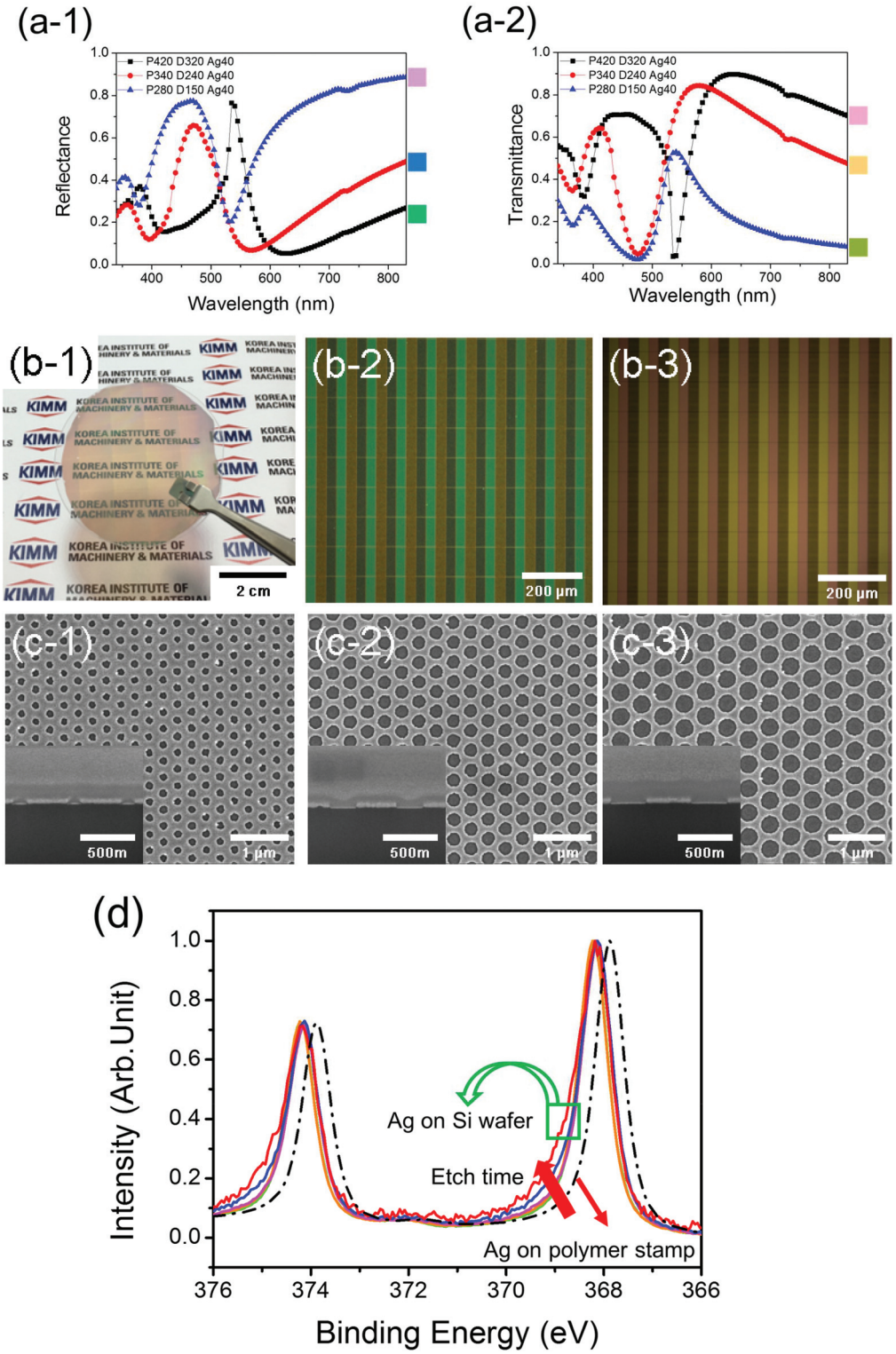


Fig. 4 Simulation and experimental results for a plasmonic color filter fabricated using MiNP. Simulated spectrum and colors of the designed color filter in (a-1) reflectance and (a-2) transmittance modes in the visible range. (b-1) Photograph of the fabricated color filter made of a Ag nanohole array on a 2 inch glass wafer. Optical microscopy images in (b-2) reflectance and (b-3) transmittance mode. (c) Surface and cross-sectional FIB images of transferred Ag nanohole arrays. (d) XPS profile of the normalized binding energy of Ag as a function of etching time through the sample.

This journal is © The Royal Society of Chemistry 2019

Published on 26 April 2019. Downloaded by Korea Advanced Institute of Science & Technology / KAIST on 11/21/2022 1:33:02 PM.

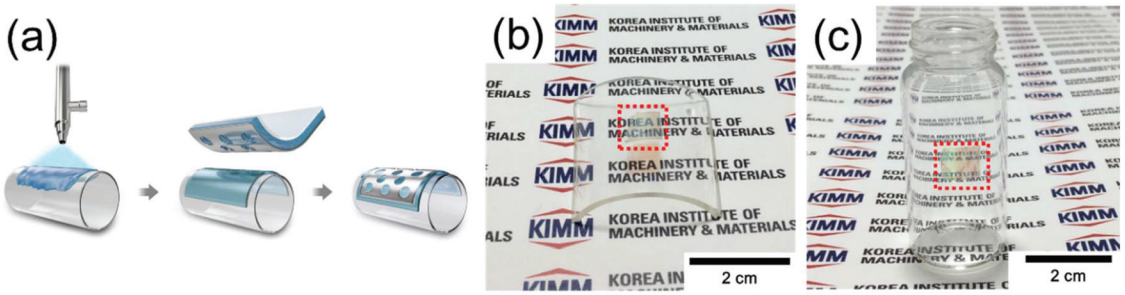


Fig. 5 Method for depositing patterns on curved surfaces. (a) Schematic illustration of the MiNP procedure for curved surfaces. Ag color filter fabricated on a (b) curved acryl surface and (c) glass vial.

decrease. NIM has been employed to fabricate large-area plasmonic color filters as it is simple and cost effective,[54] where such devices have demonstrated the feasibility of this method for fabricating nano- and microstructures. However, the problems with non-uniform residual layers should be addressed. The nTP method has also been used to fabricate plasmonic color filters,[55] although an additional thin Au layer was required between the stamp mold and deposited materials in order to effectively detach the materials from the stamp mold. Nanostructures of dielectric materials could produce more pure and vivid colors than metal-based structures.[56,57] However, in this study, we focused on demonstrating color filters made of metal using MiNP in order to provide information about the precision and stability of the fabrication process for nano and microstructures and observability with the naked eye. In addition, metallic structures have advantages for applications exploiting optical loss, such as perfect absorber.[58] From this point of view, using the MiNP method, we successfully fabricated a metallic plasmonic color filter (Fig. S13†) composed of nanohole arrays using the well-known extraordinary optical transmission (EOT) phenomenon[59,60] on both flat and curved glass substrates. A significant advantage of nanohole arrays of plasmonic color filters is that they are not affected by polarization of the light source, unlike grating arrays of color filters.[53] In this study, Ag was chosen to fabricate the color filter as it has a higher conductivity than Au and better resistance to oxidation under ambient air than Al.[61,62] To realize the red, green, and blue colors required in the filter structure, nanohole arrays with different hole sizes and pitches were designed using FDTD software for the reflectance and transmittance modes, as shown in Fig. 4(a) and (b) and Fig. S13.† The general procedure for producing the color filter was similar to that used for transfer of a line pattern (Fig. 1). Ag was deposited with a thickness of ~40 nm on the prepared polymer stamp with a hexagonal nanohole array and transferred to the adhesive-coated substrate without any defects. Fig. 4(b-1)–(b-3) show microscopy images of the transferred Ag nanohole arrays with different diameters and pitches. We verified that the top Ag nanohole arrays in contact with the adhesive were successfully transferred from the polymer stamp to the substrate, while the Ag in the trenches remained on the polymer stamp (Fig. 4(c) and Fig. S14†). In addition, optical microscopy images were used to evaluate the colors from the fabricated color filter in both reflectance and transmittance modes, and the simulation in Fig. 4(a) and the experimental images agreed well (Fig. 4(b-2) and (b-3)). This slight difference was due to the different light sources; a broadband white light source was used for the simulations, while a halogen lamp was used as the light source for experiments.

The mechanism for fabricating the nanohole array for the plasmonic color filter is expected to be similar to that for nanowire patterns (Fig. S15†). As shown in Fig. 4(d), the FWHM of the $Ag3d_{5/2}$ XPS peak (binding energy of 0.91 eV) at the interface between the transferred Ag and the adhesive layer is broader than those for the Ag on the top of the transferred nanohole array (0.72 eV) and on the polymer stamp (0.73 eV). This peak broadening is caused by the oxidation of Ag at 150 °C and the subsequent covalent bonding and formation of Ag_2O.

An important advantage of the MiNP method is that it can be applied to various applications that require curved substrates, such as sensors embedded in contact lenses or eyeglasses with an integrated meta-lens. To transfer the Ag nanohole array, as shown in Fig. 5(a), spray coating was performed for 10 s to apply the adhesive layer to an arch shape made of acryl (Fig. 5(b) and Fig. S16†) and a glass vial (Fig. 5(c)). Following the same transfer procedure, a Ag nanohole array was successfully transferred to both curved substrates, indicating that the MiNP method is viable for use with substrates of various shapes and materials.

4. Conclusion

We successfully demonstrated a repeatable MiNP method for easily transferring nanopatterns of Au, Ag, and Al over a large area without additional processes. It is notable that this method is based on the oxidation of nanoscale metal structures at 150 °C and natural oxidation during deposition, resulting in strong covalent bonding between the oxidized metals and oxygen or silicon in the adhesive layers. The strong covalent bonds formed *via* instantaneous reactions allow various metal layers to be easily detached from the polymer stamp and transferred to the substrate. We demonstrated that

Published on 26 April 2019. Downloaded by Korea Advanced Institute of Science & Technology / KAIST on 11/21/2022 1:33:02 PM.

100 nm *L*/*S* patterns of Ag, Au, and Al (with various orientations) could be quickly and easily transferred to both glass and Si substrates and the various patterns could be sequentially applied to the same substrate. In addition, the stitch method was demonstrated using the MiNP method with different metals. XPS analyses confirmed that Ag and Au were oxidized, whereas Al (which is easily oxidized) formed covalent bonds at the interface with the adhesion layer. Finally, the experimental and simulated spectra coincided well for plasmonic color filters fabricated on both glass wafers and curved glass substrates. We propose that this simple, robust, and rapid technique is highly suitable for fabricating various patterns, regardless of the metal type. In addition, it is expected that large-area applications, such as color filters, wire grid polarizers, and contact lens with embedded sensors could be fabricated by combining the MiNP method with the stitch method.

Conflicts of interest

There are no conflicts to declare.

Acknowledgements

This work was supported by the Center for Advanced Meta-Materials (CAMM) funded by the Ministry of Science, ICT and Future Planning as Global Frontier Project (CAMM-No.2014M3A6B3063707), Sensor Industry Enhancement Program (20003125) funded by the Ministry of Trade, Industry & Energy (MI, Korea), and the Basic Research Program of KIMM (Korea Institute of Machinery and Materials, NK211B).

Notes and references

1 U. Y. Lau, S. S. Saxer, J. Lee, E. Bat and H. D. Maynard, *ACS Nano*, 2016, **10**, 723.
2 M. Horák, K. Bukvišová, V. Švarc, J. Jaskowiec, V. Křápek and T. Šikola, *Sci. Rep.*, 2018, **8**, 9640.
3 V. R. Manfrinato, A. Stein, L. Zhang, C.-Y. Nam, K. G. Yager, E. A. Stach and C. T. Black, *Nano Lett.*, 2017, **17**, 4562.
4 A. B. Taylor, P. Michaux, A. S. M. Mohsin and J. W. M. Chon, *Opt. Express*, 2014, **22**, 13234.
5 Z. Zang, X. Zeng, J. Du, M. Wang and X. Tang, *Opt. Lett.*, 2016, **41**, 3463.
6 D.-X. Lu, Y.-L. Zhang, D.-D. Han, H. Wang, H. Xia, Q.-D. Chen, H. Ding and H.-B. Sun, *J. Mater. Chem. C*, 2015, **3**, 1751.
7 S. Wang, Y. Yu, R. Li, G. Feng, Z. Wu, G. Compagnini, A. Gulino, Z. Feng and A. Hu, *Electrochim. Acta*, 2017, **241**, 153.
8 J. B. In, B. Hsia, J.-H. Yoo, S. Hyun, C. Carraro, R. Maboudian and C. P. Grigoropoulos, *Carbon*, 2015, **83**, 144.
9 S.-W. Ahn, K.-D. Lee, J.-S. Kim, S. H. Kim, J.-D. Park, S.-H. Lee and P.-W. Yoon, *Nanotechnology*, 2005, **16**, 1874.
10 M. D. Austin, H. Ge, W. Wu, M. Li, Z. Yu, D. Wasserman, S. A. Lyon and S. Y. Chou, *Appl. Phys. Lett.*, 2004, **84**, 5299.
11 S. H. Ahn and L. J. Guo, *ACS Nano*, 2009, **3**, 2304.
12 S. H. Ahn and L. J. Guo, *Adv. Mater.*, 2008, **20**, 2044.
13 J. Zaumseil, M. A. Meitl, J. W. P. Hsu, B. R. Acharya, K. W. Baldwin, Y.-L. Loo and J. A. Rogers, *Nano Lett.*, 2003, **3**, 1223.
14 D. Chanda, K. Shigeta, S. Gupta, T. Cain, A. Carlson, A. Mihi, A. J. Baca, G. R. Bogart, P. Braun and J. A. Rogers, *Nat. Nanotechnol.*, 2011, **6**, 402.
15 J. W. Jeong, W. I. Park, L.-M. Do, J.-H. Park, T.-H. Kim, G. Chae and Y. S. Jung, *Adv. Mater.*, 2012, **24**, 3526.
16 C. Stuart, H.-K. Park and Y. Chen, *Small*, 2010, **6**, 1663.
17 P. B. Catrysse and S. Fan, *Nano Lett.*, 2010, **10**, 2944.
18 T. S. Mentzel, D. D. Wanger, N. Ray, B. J. Walker, D. Strasfeld, M. G. Bawendi and M. A. Kastner, *Nano Lett.*, 2012, **12**, 4404.
19 A. Cagliani, D. M. A. Mackenzie, L. K. Tschammer, F. Pizzocchero, K. Almdal and P. Bøggild, *Nano Res.*, 2014, **7**, 743.
20 M. Mesch, C. Zhang, P. V. Braun and H. Giessen, *ACS Photonics*, 2015, **2**, 475.
21 S. Bagheri, N. Strohfeldt, F. Sterl, A. Berrier, A. Tittl and H. Giessen, *ACS Sens.*, 2016, **1**, 1148.
22 S. Cosson, L. G. Aeberli, N. Brandenberg and M. P. Lutolf, *Lab Chip*, 2015, **15**, 72.
23 J. Chen, Y. Zhou, D. Wang, F. He, V. M. Rotello, K. R. Carter, J. J. Watkins and S. R. Nugen, *Lab Chip*, 2015, **15**, 3086.
24 F. Cheng, J. Gao, T. S. Luk and X. Yang, *Sci. Rep.*, 2015, **5**, 11045.
25 S. J. Tan, L. Zhang, D. Zhu, X. M. Goh, Y. M. Wang, K. Kumar, C.-W. Qiu and J. K. W. Yang, *Nano Lett.*, 2014, **14**, 4023.
26 F. Cheng, J. Gao, L. Stan, D. Rosenmann, D. Czaplewski and X. Yang, *Opt. Express*, 2015, **23**, 14552.
27 S.-H. Hwang, M.-J. Kim, S. Jeon, B. Shin and J.-H. Jeong, *Nanotechnology*, 2018, **29**, 415301.
28 C. Vieu, F. Carcenac, A. Pépin, Y. Chen, M. Mejias, A. Lebib, L. Manin-Ferlazzo, L. Couraud and H. Launois, *Appl. Surf. Sci.*, 2000, **164**, 111.
29 E. M. Hicks, S. Zou, G. C. Schatz, K. G. Spears, R. P. Van Duyne, L. Gunnarsson, T. Rindzevicius, B. Kasemo and M. Käll, *Nano Lett.*, 2005, **5**, 1065.
30 A. Radke, T. Gissibl, T. Klotzbücher, P. V. Braun and H. Giessen, *Adv. Mater.*, 2011, **23**, 3018.
31 S. Bagheri, K. Weber, T. Gissibl, T. Weiss, F. Neubrech and H. Giessen, *ACS Photonics*, 2015, **2**, 779.
32 Y. Yao, Y. Wang, H. Liu, Y. Li, B. Song and W. Wu, *Appl. Phys. A*, 2015, **121**, 399.
33 V. Rinnerbauer, E. Lausecker, F. Schäffler, P. Reininger, G. Strasser, R. D. Geil, J. D. Joannopoulos, M. Soljačić and I. Celanovic, *Optica*, 2015, **2**, 743.

 This journal is © The Royal Society of Chemistry 2019

Published on 26 April 2019. Downloaded by Korea Advanced Institute of Science & Technology / KAIST on 11/21/2022 1:33:02 PM.

34 S. Yim, S. Jeon, J. M. Kim, K. M. Baek, G. H. Lee, H. Kim, J. Shin and Y. S. Jung, *ACS Appl. Mater. Interfaces*, 2018, **10**, 2216.
35 B. Hwang, S.-H. Shin, S.-H. Hwang, J.-Y. Jung, J.-H. Choi, B.-K. Ju and J.-H. Jeong, *ACS Appl. Mater. Interfaces*, 2017, **9**, 27351.
36 S.-H. Hur and D.-Y. Khang, *Appl. Phys. Lett.*, 2004, **85**, 5730.
37 J. W. Jeong, S. R. Yang, Y. H. Hur, S. W. Kim, K. M. Baek, S. Yim, H.-I. Jang, J. H. Park, S. Y. Lee, C.-O. Park and Y. S. Jung, *Nat. Commun.*, 2014, **5**, 5387.
38 M.-H. Seo, S.-J. Choi, S. H. Park, J.-Y. Yoo, S. K. Lim, J.-S. Lee, K.-W. Choi, M.-S. Jo, I.-D. Kim and J.-B. Yoon, *ACS Nano*, 2018, **12**, 4387.
39 R. F. Tiefenauer, K. Tybrandt, M. Aramesh and J. Vörös, *ACS Nano*, 2018, **12**, 2514.
40 S. H. Hwang, S. Jeon, M. J. Kim, D.-G. Choi, J.-H. Choi, J.-Y. Jung, K.-S. Kim, J. Lee, J. H. Jeong and J. R. Youn, *Nanoscale*, 2017, **9**, 14335.
41 K. Du, I. Wathuthanthri, Y. Liu, W. Xu and C.-H. Choi, *ACS Appl. Mater. Interfaces*, 2012, **4**, 5505.
42 S. Gilles, S. Winter, K. E. Michael, S. H. Meffert, P. G. Li, K. Greben, U. Simon, A. Offenhausser and D. Mayer, *Small*, 2012, **8**, 3357.
43 A. Vohra, R. S. Carmichael and T. B. Carmichael, *Langmuir*, 2016, **32**, 10206.
44 R. Ueno and B. Kim, *Microelectron. Eng.*, 2017, **171**, 6.
45 Z.-J. Zhao, S.-H. Shin, D.-G. Choi, S.-H. Park and J.-H. Jeong, *Small*, 2018, **14**, 1703102.
46 D. Wen, F. Yue, G. Li, G. Zheng, K. Chan, S. Chen, M. Chen, K. F. Li, P. W. H. Wong, K. W. Cheah, E. Y. B. Pun, S. Zhang and X. Chen, *Nat. Commun.*, 2015, **6**, 8241.
47 G. Zheng, H. Mühlenbernd, M. Kenney, G. Li, T. Zentgraf and S. Zhang, *Nat. Nanotechnol.*, 2015, **10**, 308.
48 J. F. Weaver and G. B. Hoflund, *J. Phys. Chem.*, 1994, **98**, 8519.
49 G. B. Hoflund, Z. F. Hazos and G. N. Salaita, *Phys. Rev. B: Condens. Matter Mater. Phys.*, 2000, **62**, 11126.
50 M. P. Casaletto, A. Longo, A. Martorana, A. Prestianni and A. M. Venezia, *Surf. Interface Anal.*, 2006, **38**, 215.
51 D. A. Kaplowitz, G. Jian, K. Gaskell, R. Jacob and M. R. Zachariah, *J. Energ. Mater.*, 2014, **32**, 95.
52 M. Koyama, S. Arai, S. Suenaga and M. Nakahashi, *J. Mater. Sci.*, 1993, **28**, 830.
53 Z.-J. Zhao, M. Lee, H. Kang, S.-H. Hwang, S. Jeon, N. Park, S.-H. Park and J.-H. Jeong, *ACS Appl. Mater. Interfaces*, 2018, **10**, 9188.
54 A. F. Kaplan, T. Xu and L. J. Guo, *Appl. Phys. Lett.*, 2011, **99**, 143111.
55 A. F. Kaplan, T. Xu, Y. K. Wu and L. J. Guo, *J. Vac. Sci. Technol., B: Nanotechnol. Microelectron.: Mater., Process., Meas., Phenom.*, 2010, **28**, C6O60.
56 S. Sun, Z. Zhou, C. Zhang, Y. Gao, Z. Duan, S. Xiao and Q. Song, *ACS Nano*, 2017, **11**, 4445.
57 C.-S. Park, V. R. Shrestha, W. Yue, S. Gao, S.-S. Lee, E.-S. Kim and D.-Y. Choi, *Sci. Rep.*, 2017, **7**, 2556.
58 G. M. Akselrod, J. Huang, T. B. Hoang, P. T. Bowen, L. Su, D. R. Smith and M. H. Mikkelsen, *Adv. Mater.*, 2015, **27**, 8028.
59 T. W. Ebbesen, H. J. Lezec, H. F. Ghaemi, T. Thio and P. A. Wolff, *Nature*, 1998, **391**, 667.
60 L. Martin-Moreno, F. J. García-Vidal, H. J. Lezec, K. M. Pellerin, T. Thio, J. B. Pendry and T. W. Ebbesen, *Phys. Rev. Lett.*, 2001, **86**, 1114.
61 V. G. Kravets, R. Jalil, Y.-J. Kim, D. Ansell, D. E. Aznakayeva, B. Thackray, L. Britnell, B. D. Belle, F. Withers, I. P. Radko, Z. Han, S. I. Bozhevolnyi, K. S. Novoselov, A. K. Geim and A. N. Grigorenko, *Sci. Rep.*, 2014, **4**, 5517.
62 J. H. Park, P. Ambwani, M. Manno, N. C. Lindquist, P. Nagpal, S.-H. Oh, C. Leighton and D. J. Norris, *Adv. Mater.*, 2012, **24**, 3988.